Supplementary Material for Numerical Modeling and Seismic Data

Mechanical and Thermal Equilibrium

For each numerical time step, the modelling involves direct solution of the equation of motion for every grid point including the effects of inertia:

$$\frac{\partial \sigma_{ij}}{\partial x_j} - \rho g_i = \rho \frac{\partial v_i}{\partial t} \tag{1}$$

where v_i is the velocity at each grid point, g_i is the acceleration due to gravity, ρ is the mass density and σ_{ij} is the stress in each grid element. In order to approximate quasi-static processes, the effects of inertia must be damped in a way akin to oscillations in a damped oscillator. Starting from a non-equilibrium state, the forces present at each grid point are summed ($f_i = \rho\delta v_i/\delta t$). The corresponding out-of-balance forces and the mass at the grid point give rise to acceleration. The accelerations are integrated to calculate the new velocities that are used to determine the incremental strain, ε_{ij} at each grid point. During a single time step, finite rotations also change the stress tensor, which is defined with respect to a fixed frame of reference. Before the incremental strains are determined, the stress tensor is updated to take these rotations into consideration as follows.

$$\sigma_{ij}^{new} = \sigma_{ij}^{old} + \left(\omega_{ik}\sigma_{kj} - \sigma_{ik}\omega_{kj}\right)\Delta t \tag{2}$$

where Δt is the time step and ω_{ij} , the rotation per unit time, is given in terms of the velocity derivatives by

$$\omega_{ij} = \frac{1}{2}\left(\frac{\partial v_i}{\partial x_j} - \frac{\partial v_j}{\partial x_i}\right) \tag{3}$$

By using the constitutive law for elastic, viscous and plastic rheologies, the corresponding stress increments are determined from the strain increments and the forces that they produce on the surrounding grid points are summed to determine the new out-of-balance forces and velocities. This dynamic response is then damped to approach a quasi-static equilibrium. FLAC is a very powerful technique for simulating non-linear rheological behaviour at relatively high resolution (the grid size is 1 km) because the explicit time-marching scheme does not require the storage of the large matrices that are needed for implicit methods. The time step of the calculation scales with the elastic-plastic property of our model. If the problem is purely elastic, the time step of the dynamic response scales with the velocity of the elastic wave propagating through the elements. This time step is of the order of a few hundredths of a second. Therefore, the resolution of the domains studied and the timescale needed for our numerical experiments would yield very long run times. In order to decrease the CPU time needed to perform the numerical experiments, we increase the speed of calculation by setting the boundary displacement per time step to a fraction of the grid spacing. To set the boundary displacement, we choose a ratio of boundary velocity to sound velocity of $10^{-6} – 10^{-5}$. We find that this ratio allows for fast enough runs and at the same time minimizes the error in the strain calculation.

We model the evolution of the temperature as the model material deforms by using a Lagrangian formulation. We use an explicit finite difference method as used in FLAC. For each time step, the flow of heat through each element is calculated using Fourier's law. The corresponding energy is then summed and the temperature is calculated at each grid points using the energy equation:

$$\rho C_p \frac{\partial T}{\partial t} - \nabla.(kT) = H \quad (4)$$

where T is the temperature, ρ is the density of the material, C_p is capacity calorific, k is the thermal conductivity tensor, and H is the heat production per unit volume.

Re-meshing

The initial mesh of the model is made of quadrilaterals subdivided into two pairs of superimposed constant-strain triangular zones. The use of triangular zones eliminates the problem of "hour-glassing" deformation sometimes experienced in finite differences. Since this method is Lagrangian (i.e., the numerical grid follows the deformations), the simulation of large deformation (locally more than 50%) involves re-meshing to overcome the problem of degradation of numerical precision when elements are distorted. We trigger re-meshing when one of the triangles in the grid elements are distorted enough that one of its angles becomes smaller than a given value. Every time re-meshing occurs, strains at each grid point are interpolated between the old deformed mesh and the new undeformed mesh using the barycentric coordinates of the nodes and Gauss points of the new elements in the old deformed mesh. The new state of strain is then used with the rheological laws to calculate the stress and resulting out-of-balance forces to start the time step cycle again. Also every time we re-mesh, errors in the interpolation of the state variables result in an increase in the out-of-balance force, and artificial accelerations and oscillations may occur. For this reason the solution may not be in equilibrium immediately after re-meshing. We have tested different criteria to trigger re-meshing in order to reduce the oscillations and chose to use a minimum angle of 15° before re-meshing of the grid.

Particle tracking.

To guarantee that the boundary between the different physical phases in the model (i.e, quartz, plagioclase, olivine) do not diffuse at the time of re-meshing, we use particles distributed in the grid elements. These particles have both Eulerian and Lagrangian coordinates attached to the elements. When re-meshing occurs their Eulerian and barycentric (Lagrangian) coordinates and their physical properties are registered in the old grid. When the new regular grid is formed the Eulerian coordinate of the particles are used to calculate the new barycentric coordinates of the particles in the new grid elements. Then the physical properties are then properly assigned with no spatial diffusion. These particles are also used to track the pressure, strain and temperature history of the different phased through the deformation history. New particles are added or destroyed when needed (i.e. when few particles populate one given grid element or when a particle falls out of the new mesh boundaries after re-meshing). Similar re-meshing techniques have been developed in previous work showing the efficiency of this method (*Babeyko and Sobolev*, 2008; *Burov and Yamato*, 2008; *Popov and Sobolev*, 2008)

Rheology

For ductile material, we use the Maxwell viscoelastic constitutive equations relating the deviatoric stresses to the deviatoric strains. In this formulation τ_M, the Maxwell time at which viscous deformation starts after a period of elastic strain accumulation, is defined as $t_M = 2\eta/E$ where E is the Young's modulus, η being the effective viscosity. The semi-brittle part of the crust is defined as a bimineralic rock with a strong phase (anorthosite) and a weak phase (quartz) (*Lavier and Manatschal*, 2006). We model semi-brittle fractures by the accumulation of strain (damage) in the middle crust. Where plastic strain accumulation occurs over a certain threshold, we assume that the shear zones become ductile by changing the rheology from that of anorthosite to quartz. Yield is initiated for an amount of work corresponding to 4.e6 J between temperatures of 300ºC and 450ºC corresponding to the onset of plasticity for quartz and the onset of plasticity for plagioclase (*Lavier and Manatschal*, 2006). Since anorthosite is brittle for a temperature as high as 450°C, the middle crust is brittle at greenschist to amphibole facies condition, which corresponds to the initial temperature conditions in the crust in the Pyrenean-Bay of Biscay system. When strain (elasto-plastic or visco-elastic deformation) accumulates in the middle crust, we assume that a weak phase, chosen as wet quartz, replaces anorthosite in the shear fracture. Also, after the initiation of the fracture, for a small amount of elasto-plastic or ductile strain (3 %), we accumulate weak quartz in the fractured zone that will then flow in a visco-elastic manner (ductilely). This leads to the progressive formation of ductile shear zones in the models that act as semi-brittle fracture. This process is similar to what is described in the field for the formation and evolution of ductile shear zones (*Manktelow and Pennachioni, 2005*).

The main assumption of our models is that the type of fracture observed in the semi-brittle crust is resulting from the accumulation of plastic work. By plastic work, we mean any inelastic work accumulation in the semi-brittle media. This can be brittle plastic or viscous strain accumulation. We use a simple yield criterion based on Freudhental's critical plastic work criterion (*Freudhental*, 1950) that depends on both the square root of the second invariant of stress, σ^{II} and strain, ε^{II} (also called Mises stress and strain) to simulate the formation of fracture as a function of plastic and viscous work (i.e. semi-brittle fracture):

$$\int_0^{\varepsilon_c} \sigma^{II} \varepsilon^{II} d\varepsilon = C \qquad (5)$$

Where ε_c is the critical strain at which fracture occurs and C is a constant set at 4.10^6 J to initiate semi-brittle fracture at high stresses, $\sigma^{II} = 4.10^8$ Pa for low strains ($\varepsilon_c = 0.01$) and at low stresses $\sigma^{II} = 4.10^6$ Pa for high strains ($\varepsilon_c = 1$). For this range of parameters, fracture can both initiate in the brittle crust for high stress environments and in the ductile crust for low stress environments. In the models presented here, we are concerned only by the evolution of deformation over thousands to millions of year. At this time scale nucleation of the shear zones is instantaneous and we can assume that the stresses are constant over the time of damage and nucleation. The yield criterion becomes:

Error! Bookmark not defined.Error! Bookmark not defined.

$$\sigma^{II}\varepsilon_c = C$$
with
$$\varepsilon_c = \varepsilon_c^{elastoplastic} + \varepsilon_c^{viscoelastic} \qquad (6)$$

$\varepsilon^{elastoplastic} \approx \sigma^{II}_{Mohr} / E$ where σ^{II}_{Mohr} is the square root of second invariant of stress at the Mohr-Coulomb failure criteria and E is Young´s modulus. $\varepsilon^{viscoelastic} \approx \sigma^{II}_{creep} / C$ where σ^{II}_{creep} is the square root of the second invariant of the dislocation creep yield stress and C the viscosity at yield.

When assuming pressure dependent**Error! Bookmark not defined.** Mohr-Coulomb plastic behaviour for the brittle crust and viscous creep for the ductile crust, one can plot the yield stress envelope as a function of depth for a given geotherm in the classical Christmas tree shape (e.g., *Kholstedt, et al.,* 1995). We showed that yield stress for semi-brittle fractures is dependent on critical work and accumulated strain. We can extend the principle of the yield stress envelope by plotting the ductile fracture criterion as yield stress as a function of total strain (Fig. DR1). To have a consistent yield stress between Mohr-Coulomb, viscous creep and ductile fracture we calculate the Mises stress, σ^{II} for Mohr Coulomb and viscous creep at yield. Mohr Coulomb shear stress, τ at yield is defined as:

$$\tau = \mu\sigma_n \qquad (7)$$

Where σ_n is the normal stress, μ the friction coefficient. In 2D the second invariant of the stress at yield is defined as a function of the principal stresses as:

$$\sigma^{II}_{yield} = \sqrt{\sigma_1^{yield}\sigma_3^{yield}} \qquad (8)$$

or as a function of shear stress at yield, with $\sigma_n = \frac{\sigma_1 + \sigma_3}{2}$ and $\tau = \frac{\sigma_1 - \sigma_3}{2}$.

$$\sigma_{yield}^{II} = \sqrt{\tau^2 \left(\frac{1-\mu}{\mu} \right)} \tag{9}$$

For viscous creep the second invariant at yield is defined as follow:

$$\sigma_{yield}^{II} = A^{\frac{1}{n}} \left(\dot{\varepsilon}^{II} \right)^{-\frac{1}{n}} e^{\frac{Q}{nRT}} \tag{10}$$

where A is the creep law pre-exponent, Q the activation energy, $\dot{\varepsilon}^{II}$ the square root of the second invariant of the strain rate, n the creep law exponent, R the gas constant and T the temperature. Finally, the yield for semi-brittle fracture is defined as:

$$\sigma^{II} = \frac{C}{\varepsilon^{II}} \tag{11}$$

We plot yield stresses as a function of depth (Supplementary Fig. DR1) for a friction coefficient of 0.6 and a dislocation creep law for plagioclase for a constant strain rate of $\dot{\varepsilon}^{II} = 10^{-14}$ s^{-1}, a linear geotherm of 13.3 °C/km (400 °C at 30 km depth) and $C = 4.10^6$ J, a value that corresponds to a yield at a stress of 400 MPa for a strain of 1%. The defined rheology develops quasi-static fractures or veins at or near the brittle ductile transition that coalesce into ductile shear zones. In the brittle part of the crust these zones form as shear fractures following the Mohr-Coulomb orientation for localization. In the ductile crust the fractures form in the direction of the minimum principal stress. Both types of fractures are then deforming in a ductile manner after a time, t_M corresponding to the initial elastic response of a Maxwell body.

Models

We use the code PARAVOZ developed by Yuri Podlatchikov and Alexei Poliakov (*Poliakov et al.*, 1993). This version is extended to account for energy conservation and particle phase and properties tracking to reduce phase boundary diffusion in between re-meshings after large amounts of deformation (*Lavier and Buck*, 2002; *Lavier and Manatschal*, 2006). Supplementary figures DR3 to DR5 show a more detailed evolution of the model presented in figure DR3 of the main paper. In addition to the phase field, the square root of the second invariant of the strain rate and the viscosity in the model are shown (Supplementary Fig. DR3 to DR5). Each field is overlaid by a contour-plot of the boundaries between the phases. The strain rate shows the evolution of the active fault during the formation of the rift and the wedge. The viscosity shows areas of elasto-plastic behavior (from red to green 10^{23} Pa.s) and visco-elastic behavior (from green to blue 10^{20} Pa.s). The bottom plot is the density in the whole models with the corresponding topography on top. Following the models of subduction previously developed with the same numerical technique (Gurnis et al., 2004), subduction is initiated and maintained by the presence of a very weak slab interface with a coefficient of friction less the 0.02.

REFERENCES

Babeyko A.Y and S.V. Sobolev (2008), High-resolution numerical modeling of stress distribution in visco-elasto-plastic subducting slabs, Lithos, 103, 205–216.

Burov E.and P. Yamato (2008), Continental plate collision, P–T–t–z conditions and unstable vs.stable plate dynamics: Insights from thermo-mechanical modelling, Lithos 103 (2008) 178–204.

Freudenthal, A. M. (1950), The inelastic behaviour of engineering materials and structures, in *Journal of the Franklin Institute*, edited by John Wiley (New York),Volume 250, Issue 6, 584-585.

Gurnis, M., Lavier, L. L., and C. Hall, Evolving force balance during incipient subduction, Gcubed, Geochemistry, Geophysics, Geosystems, 5, Q07001, doi:10.1029/2003GC000681, 31 pp., 2004.

Jammes, S., L. Lavier, G. Manatschal,, Extreme crustal of the Bay of Biscay andWestern Pyrenees: From observations to Modeling. *Geochem. Geophys. Geosyst.*, *11*, Q10016, doi:10.1029/2010GC003218, 2010.

Kirby, S. H. and A. K. Kronenberg (1987), Rheology of the lithosphere: Selected topics, *Rev. Geophys.*, *25*, 1219-1244.

Kohlstedt, D. L., B. Evans, and S. J. Mackwell (1995), Strength of the lithosphere: Constraints imposed by laboratory experiments, *Journal of Geophysical Research*, 100(B9), 17,587–17,602.

Lavier, L. L., and W. R. Buck (2002), Half graben versus large-offset low-angle normal fault: Importance of keeping cool during normal faulting, *J. Geophys. Res.*, 107(B6), 2122, doi:10.1029/2001JB000513

Lavier, L. L., G. Manatschal, A mechanism to thin the continental lithosphere at magma poor margins , Nature 440, 324-329, 2006.

Mancktelow, N. S. and G. Pennacchioni (2005), The control of precursor brittle fracture and fluid-rock interaction on the development of single and paired ductile shear zones, *Journal of Structural Geology, 27 (4), 645-661*.

Poliakov, A.N.B, Yu Podladchikov, and C. Talbot (1993), Initiation of salt diapirs with frictional overburdens: numerical experiments *Tectonophysics, 228 (3-4), 199-210*.

Popov A.A. and S.V. Sobolev (2008), SLIM3D: A tool for three-dimensional thermomechanical modeling of lithospheric deformation with elasto-visco-plastic rheology, Physics of the Earth and Planetary Interiors, 171, Issues 1-4, p 55-75.

Ranalli, G. (1995), Rheology of the Earth, 2nd ed., 436 pp., Chapman and Hall, London.

SUPPLEMENTARY FIGURES

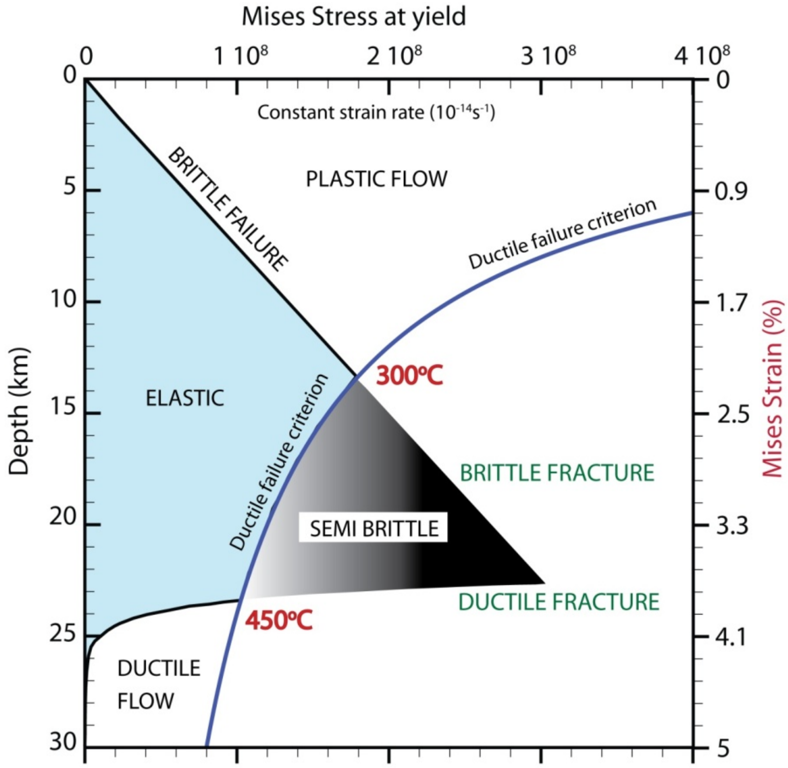

Figure DR1. We plot the square root of the second invariant of the yield stress for Mohr-Coulomb, dislocation creep and semi-brittle fracture. We show that the Yield stress of the crust is not only dependent on the normal stress, temperature and strain rate but also on the second invariant of the strain at yield (elasto-plastic and visco-elastic) that is equivalent to a measure of damage in the rocks. The resulting deformation in the lithosphere is therefore dependent on the amount of damage accumulated in the middle to lower crust. This process must be facilitated by hydro-fracturing in the presence of aqueous fluid in the crust and lithosphere.

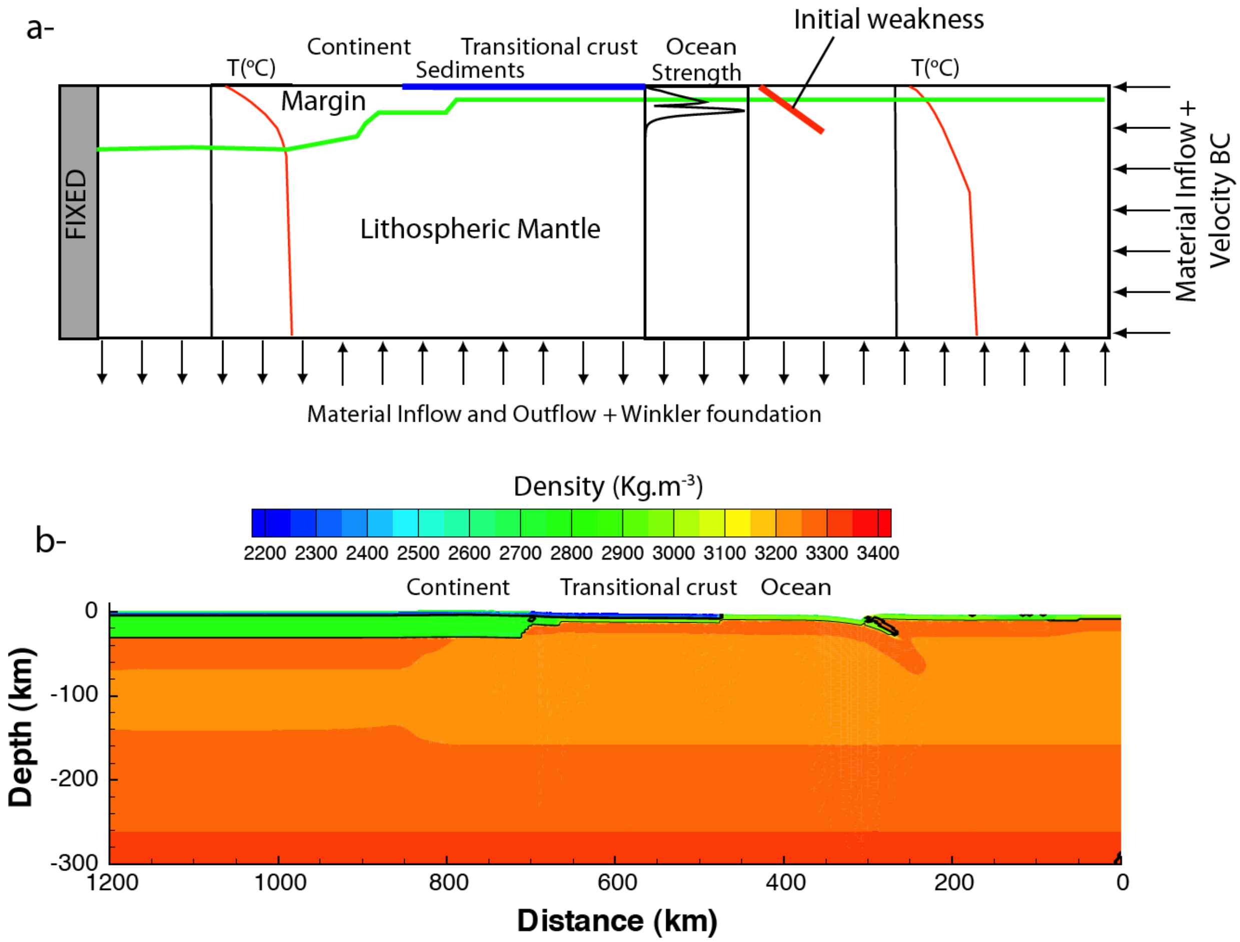

Figure DR2. The numerical code is an extended version of the model PARAVOZ (Yuri Podlatchikov, Alexei Poliakov) (Cundall, 1989; Poliakov et al., 1993; Lavier and Buck, 2002; Lavier and Manatschal, 2006; Jammes et al, 2010) that contains Eulerian-Lagrangian particles to track phase boundaries of the material transported during the brittle and ductile processes simulated in the model. The model box size is 300 km deep and 1200 km wide. The grid size is 2x4 km in the low resolution parts of the models and set at 2x2 km in the area where collision occurs. The initial geometry of the model is that of a low-resolution passive margin (to the left) and an oceanic plate (to the right). The continent (equivalent to Eurasia) is 400 km wide with a 30 km thick crust thinning to 12 km over 50 km. The transition from continent to ocean is defined as a zone of thin transitional crust (200 km x 8 km thick). A 400 m thick layer of sediments is covering the oceanic crust and a 4 km thick layer of sediments covers the margin. A zone of pre-deformed and pre-weakened oceanic crust and mantle is set to the left of the arc to initiate subduction there. The thermal age is initially set by calculating a continental geotherm over the thickness of the lithosphere corresponding to a given age after the end of the last tectonic event (Lavier and Steckler, 1997). Eclogite transformation of the oceanic crust occurs when oceanic crust reaches the depth of 50 km. The density at 273°C of the oceanic crust is increased by 350 $Kg.m^{-3}$. Serpentinization of the mantle occurs when the subducting oceanic crust is in contact with the mantle at a depth lower than 50 km, The density at 273°C is then decreased by 300 $Kg.m^{-3}$. An algorithm then transforms 2 to 3 elements above the subducting oceanic crust to serpentinized mantle with a weak olivine rheology (we decrease the activation energy of dry olivine by one order of magnitude) and a lower density (Table DR1). The collision is imposed kinematically by allowing flux of oceanic lithosphere at 5 cm yr-1 on the right side of the box. The flux at the bottom boundary is controlled by a Winkler foundation that simulates isostatic equilibrium. Table DR1 gathers the physical properties used to model the lithosphere. To localize deformation in the crust the friction coefficient is decrease from 0.6 to 0.1 and the cohesion from 44 to 4 MPa. The creep viscosities of the continental, oceanic crust and the lithospheric mantle are controlled by dislocation creep laws (equation 10).

Table DR1:

Parameter	Symbol	Value			
Rheological parameters					
Friction coefficient	μ	0.6-0.3			
Cohesion		44MPa-4MPa			
		Crust: Quartz[1]	*Crust:Plagioclase*[2]	*Gabbroic lower crust*[1]	*Mantle: Dry olivine*[1]
Power-law exponent	A	$5\ 10^{2}$ MPa^{-n}.s^{-1}	$3.3\ 10^{-4}$ MPa^{-n}.s^{-1}	$1.25\ 10^{-1}$ MPa^{-n}.s^{-1}	$7\ 10^{4}$ MPa^{-n}.s^{-1}
Activation energy	Q	$2\ 10^{5}$ J.mol^{-1}	$2.38\ 10^{5}$ J.mol^{-1}	$3.5\ 10^{5}$ J.mol^{-1}	$5.2\ 10^{5}$ J.mol^{-1}
Initial constant	n	3	3.2	3.05	3
Universal gas constant	R	8.3144 J.mol^{-1}.°C^{-1}			
Thermal parameters					
Crustal conductivity		2 W^{-1}K^{-1}			
Mantle conductivity		3.3 W^{-1}K^{-1}			
Heat production crust		10^{-9}W.Kg^{-1}			
Moho temperature		500°C			
Asthenosphere temperature		1330°C			
Thermal expansion coefficient		3.10^{-5}K^{-1}			
Surface temperature		10°C			
Densities					
Crustal density at 273°C		2800 kg.m^{3}			
Mantle lithosphere density at 273°C		3300 kg.m^{3}			

[1](*Kirby and Kronenberg, 1987*)
[2](*Ranalli, 1995*)

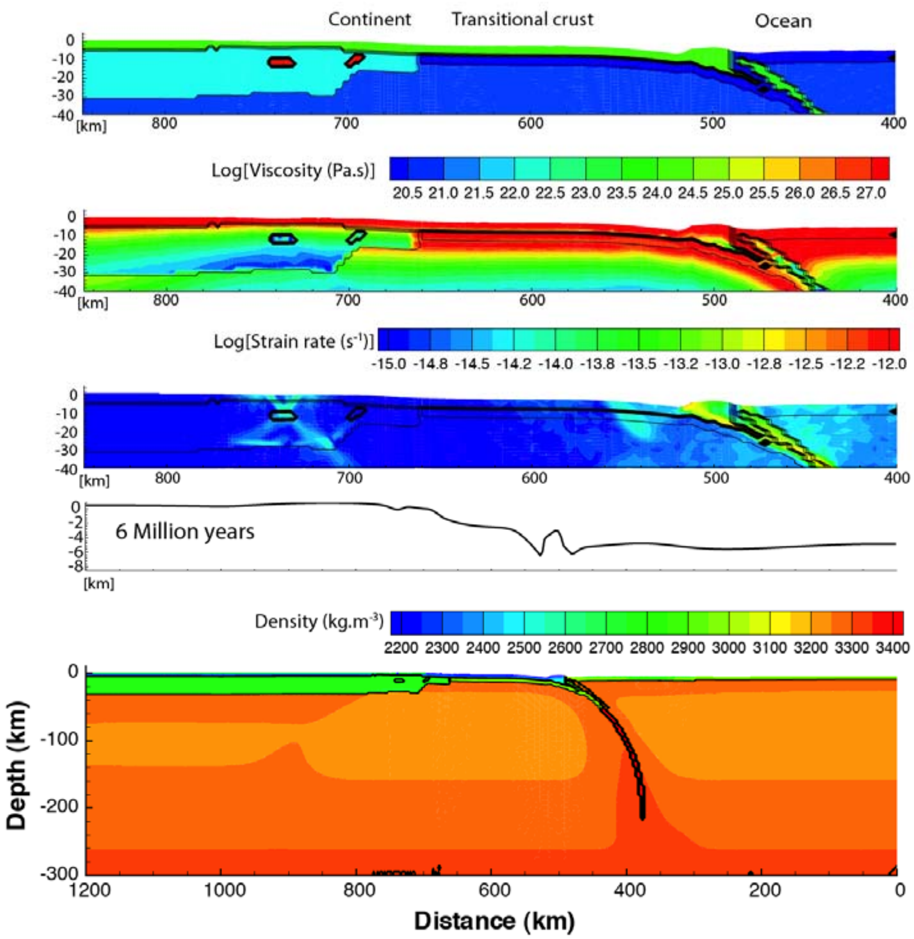

Figure DR3: Evolution of the subduction to collision after 6 million years.

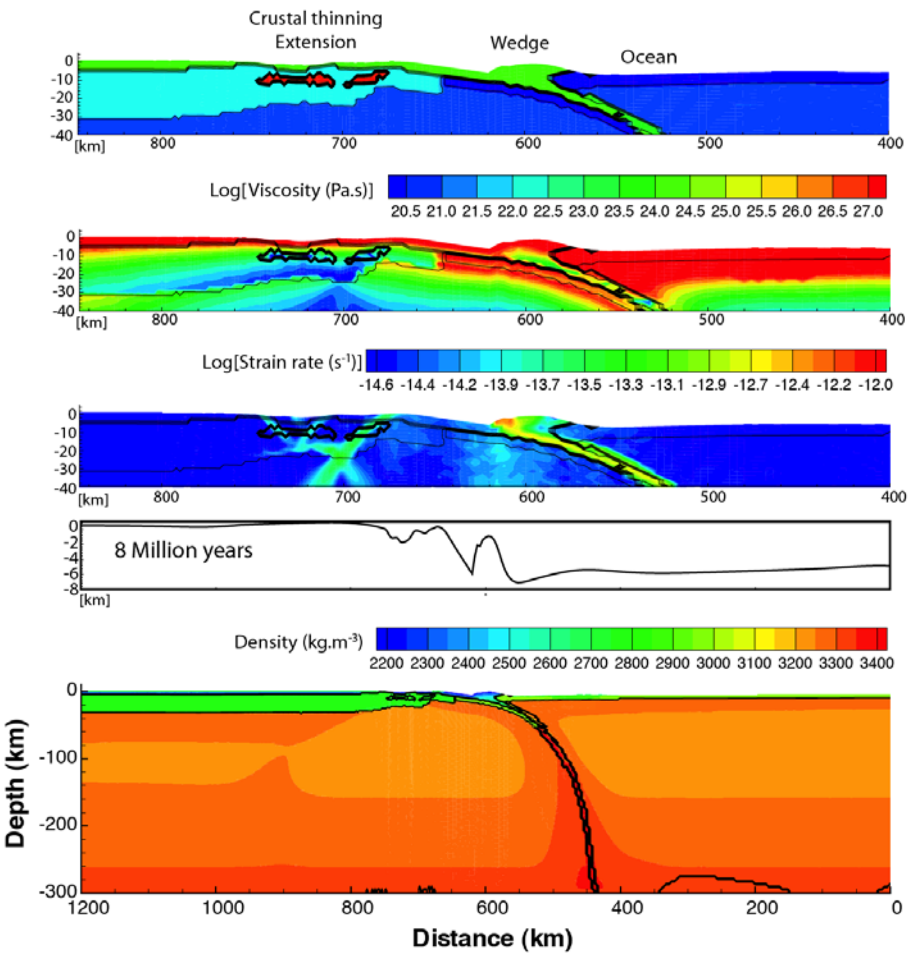

Figure DR4: Evolution of the subduction to collision after 8 million years.

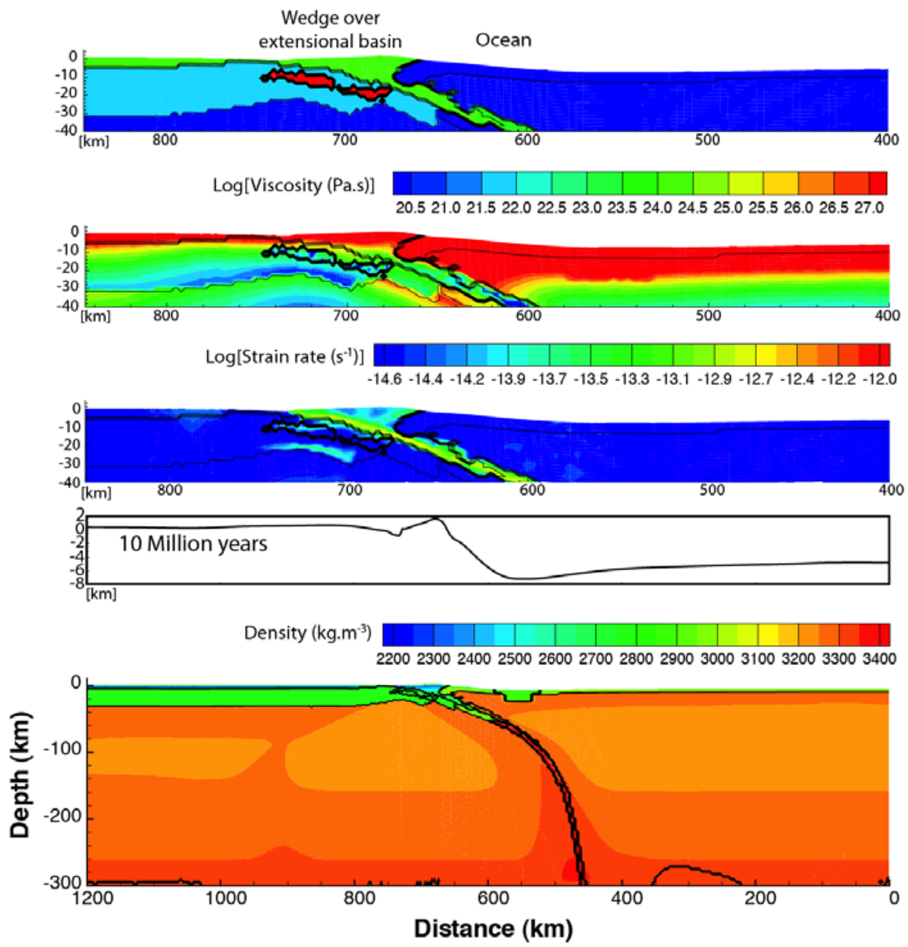

Figure DR5: Evolution of the subduction to collision after 10 million years

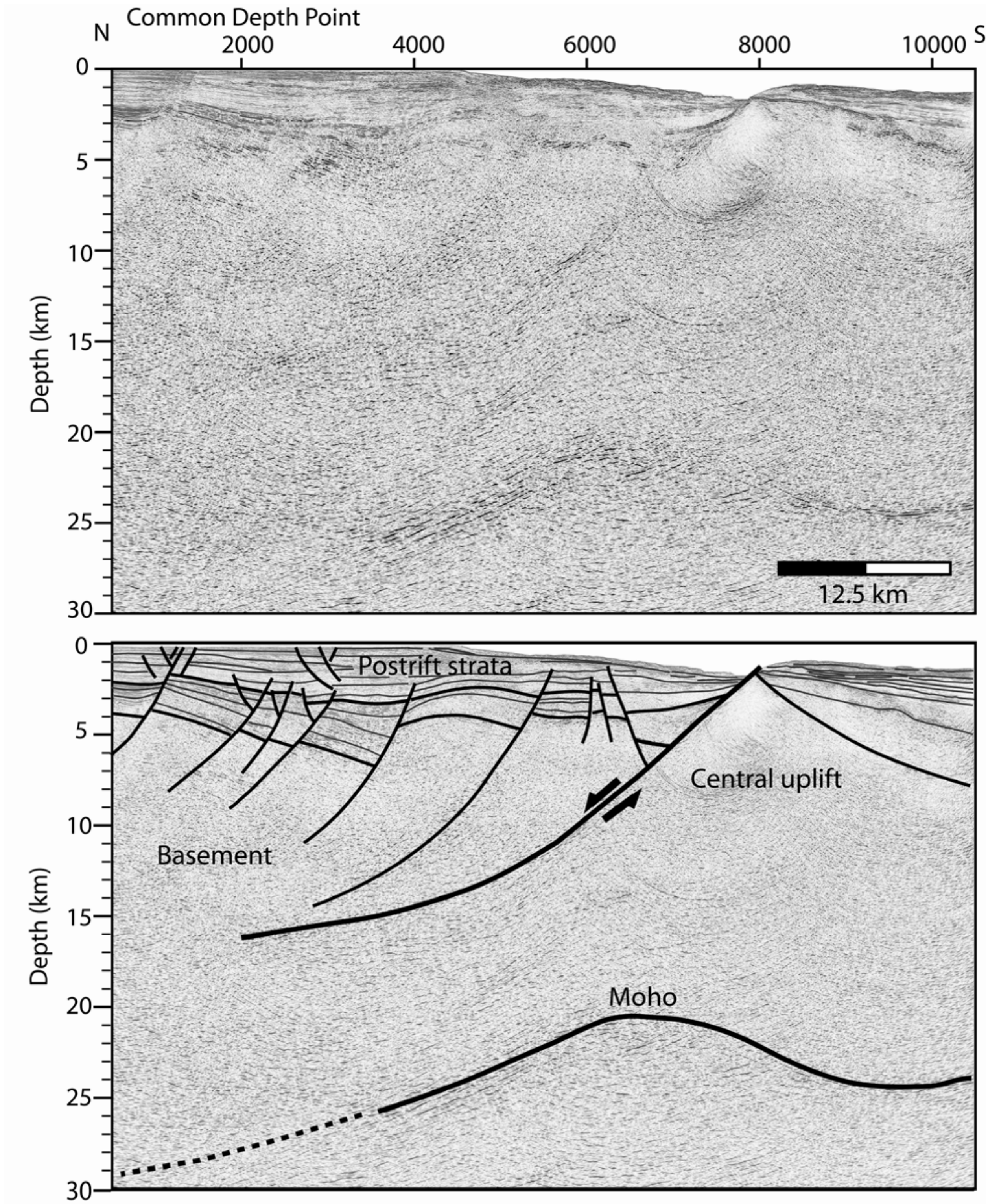

Fig. DR6: Blow-up of seismic image and interpretation in fig. 2 in text.